TOWARDS AUTONOMOUS LONG-RANGE NAVIGATION 'ISAIRAS 2005 CONFERENCE', MUNICH, 5-8 SEPTEMBER 2005

Erick Dupuis, Pierre Allard, Joseph Bakambu, Tom Lamarche, Wen-Hong Zhu, Ioannis Rekleitis

Canadian Space Agency, Space Technologies 6767 route de l'Aéroport, St-Hubert (Qc), J3Y 8Y9, Canada Email:firstname.lastname@space.gc.ca

ABSTRACT

The recent success of NASA's Mars Exploration Rovers has demonstrated the important benefits that mobility adds to landed planetary exploration missions.

The Canadian Space Agency (CSA) has been conducting research in ground control and in autonomous robotics for several years already. One of the target applications is planetary exploration using mobile platforms. The emphasis of our research program is on reactive on-board autonomy software and long-range rover navigation.

This paper describes recent activities of the CSA in this area. Key results are described in the areas of terrain modelling, path planning and rover guidance.

1 INTRODUCTION

The recent success of the Mars Exploration Rovers "Spirit" and "Opportunity" has demonstrated the important benefits that mobility adds to landed exploration missions. planetary The announcement by NASA to increase its activities in planetary exploration (via Moon and Mars missions) and the ESA Aurora program will certainly result in an increase in the number of robotic vehicles roaming on the surface of other planets. The current state-of-the-art in control of planetary rovers requires intensive human involvement throughout the planning portion of the operations [5]. Unless the terrain is relatively easy to navigate, rovers are typically limited to traverses on the order of a few tens of meters. Recently, the Mars Exploration Rovers "Spirit" and "Opportunity" have managed to conduct traverses on the order of 100 meters per day.

Although the terrains in which these traverses were accomplished were relatively free from obstacles, this is already quite an achievement. However, to increase the science return and minimise operations costs, future planetary missions will undoubtedly require the ability to traverse even longer distances autonomously. One of the key technologies that will be required to succeed towards the ambitious objectives that are being set

internationally will be to streamline the operations of future space missions.

To address this requirement, many laboratories are currently pursuing autonomous navigation of rovers for planetary exploration. Several teams approach the problem of long-range navigation through a succession of short-range traverses. Typically, the rover performs a traversability analysis of the terrain in the immediate vicinity of the rover, picks a local path that is obstaclefree and moves the rover towards the target destination (or way point) [10][15]. In contrast to this approach, a behaviourist implementation has been successfully demonstrated on a rover in a desert environment [11]. Despite the fact that only simple navigation behaviours were used, the robot successfully performed traverses up to 1.3 km in natural settings with way points spaced up to 200m apart while using a very limited sensor suite for environment sensing. In addition, some work has been done on instrument placement to reduce the level of human involvement necessary to position a scientific instrument on a target area of interest [13]. In contrast with the previous approaches some research is conducted to increase autonomy by performing basic paradigm shifts. Examples of such research are the inclusion of on-board planning and re-planning capability [5] or localisation schemes targeted specifically at long-range navigation [7]. Furthermore, it is worth noting that during last years the contestants in the DARPA Grand Challenge, vehicles with far superior capabilities of the planetary rovers were able to traverse only a small fraction of the target trajectory; a fact that highlights the difficulties of long range navigation.

The Canadian Space Agency (CSA) has been conducting research in ground control and in autonomous robotics for several years already. One of the target applications is planetary exploration using mobile platforms. The emphasis of our research program is on reactive on-board autonomy software and long-range rover navigation. This paper describes recent activities of the CSA in this area. Particular emphasis is put on terrain scanning and modelling, path planning in natural settings and rover guidance.

Experimental results from the summer 2004 test campaign are presented.

2 TERRAIN MODELLING

Range imaging is a reliable and simple way to extract accurate three-dimensional data of objects and environments. With readily available range sensors, it is understandably becoming a very popular technology for 3D modelling. Range sensing is, in our case, the data source to our terrain modelling algorithms, the first step of the long-range navigation scheme. The sensor used in our laboratory is an ILRIS-3D LIght Detection And Ranging (LIDAR) sensor commercially available from Optech Inc. This scanner uses TOF (Time-Of-Flight) principle to measure depth data on two axes. That is, a single scan provides a complete "image" of the scanned area, not just a line. Although it is not optimised for ranges under ~10 meters, its ability to gather data ranging from half a meter to more than a kilometre away makes it well adapted to long-range considerations. Specifications in a nutshell are: eyesafe IR laser, data sample rate of 2000 points/second, ±20° field-of-view on both axes, modelled output accuracy in the 5mm range and a maximum angular resolution of 26x10⁻⁶ radians (2.6mm spacing at 100m).



Figure 1 - Scan of the Mars yard (CSA building in background)

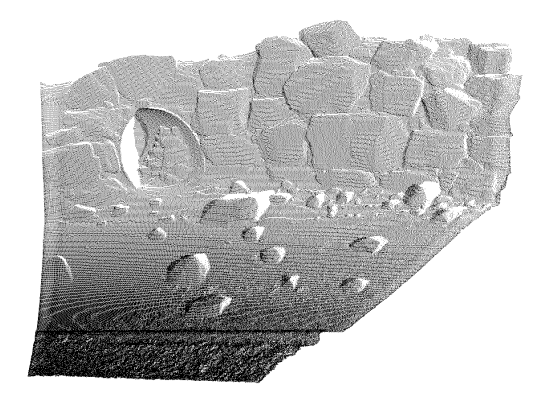


Figure 2 - Scan of the Mars yard cliff

Data returned by the ILRIS-3D is a point cloud expressed as a list of three-dimensional coordinates in the scanner's reference frame. For navigation in a planetary exploration scenario, analysis was conducted to establish the most appropriate data structure to map unknown and unstructured environments.

2.1 Meshing

Since a point cloud is not an appropriate structure to plan navigation, an irregular triangle mesh structure was chosen. One of the main advantages of the triangular irregular mesh over classical digital elevation maps (DEM) is that it inherently supports variable resolution. This allows modelling precise details of uneven areas while simplifying flat areas to just a few triangles, therefore minimising the overall memory requirements. Variable resolution could also be accomplished by the quad-tree representation, a cousin of the DEM. Unfortunately, quad-trees introduce a loss of precision because the acquired data points get approximated by square areas. Moreover, a small change in the data (a small shift in an area) could mean reprocessing the complete data set thus, making their use very time intensive. Adding to that, both DEM and quad-trees are 2.5D representations. Therefore, they do not support concave geological structures like overhangs and caverns, which pose no problem to irregular triangular meshes.

Once a static LIDAR scan is taken, we generate the initial high-resolution mesh from the data points. Triangulating a set of general three-dimensional points presents many difficulties like, for example, determining neighbour points that define a common surface on the real object. To avoid such problem, we take advantage of a property inherent to range sensing devices, namely 2.5D data. As a matter of fact, even though we tend to say these sensors provide 3D points, a single scan will in reality always be a set of 2.5D data. Even though you may get Cartesian data (x, y, z) from the range sensor, it is converted from the original measurements made in a spherical coordinates system (θ, ϕ, r) defining respectively azimuth, elevation and radius (distance). Data of one scan in this coordinate system is 2.5D, with only one radius (r) value corresponding to any angular position set (θ, ϕ) . That means that neighbours in the θ - ϕ plane are necessarily neighbours in reality (discontinuity may exist, but will be handled later by the shadow removing algorithm). From there, we compute the Delaunay triangulation of the points projected in the 2D θ - ϕ plane. This is done by temporarily generating emulated "r" values for every point according to the equation below, which produces a paraboloid of revolution.

$$r = \theta^2 + \phi^2$$

The resulting emulated surface is fed into a 3D convex hull algorithm [9]. The lower part of the returned hull is the Delaunay triangulation of the data points projected in the θ - ϕ plane. Projecting this 2D triangulation back on the original coordinates gives us our initial mesh. It is worth noting that once projected on the original data, the triangulation may not hold its Delaunay properties anymore (min-max and empty-circle criterions).

We now have a mesh that does not present any holes, even though the real surface "seen" by the LIDAR usually has some discontinuities due to the sensor's low angle of incidence (Figure 4). These shadow regions exist whenever there is an object in front of another. Triangles covering these shadow regions must be identified and removed from the mesh because they do not model an existing surface.

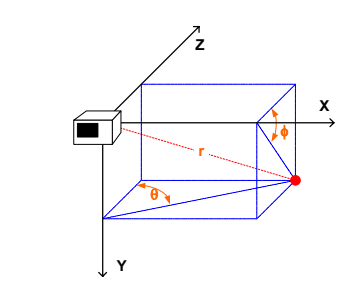


Figure 3 - ILRIS-3D reference frame

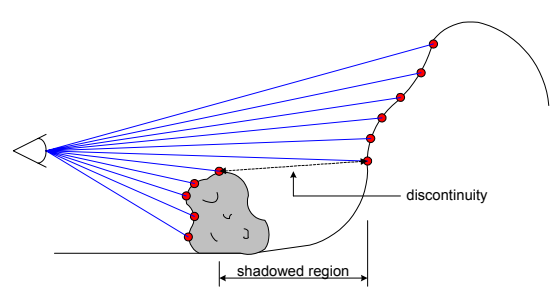


Figure 4 - "Shadows"

2.2 Shadow filtering

Two consecutive algorithms are used to remove the "shadow" triangles. The first one, doing most of the job, is based on the coefficient of variance (CV) of the triangles' vertices distance (r). For every triangle we have in the mesh, we compute the average distance (r_{mean}) and standard deviation (s) of its vertices' length. Coefficient of variance then provides a normalized representation of the distance variability among these three vertices (2). That is, triangles having their three vertices near one another will have a low CV while elongated triangles (presumably shadow triangles) will have higher CV.

$$CV = \frac{s}{|r_{mean}|} \times 100$$

The CV threshold to apply will depend on the scanning resolution. For example, empirical testing showed that a threshold of 8% resulted in reasonable filtering of the shadows for scan steps around 0.26° while 4% was adequate for a higher resolution of 0.16° steps (Figure 5: down-sampled data of Figure 1 without the background buildings). Note here that this filtering also has the effect of removing the unwanted triangles generated by outlier points, if any. In some cases, there will also be unwanted large triangles linking points located at the extremity of the scan. This makes sense from the convex hull algorithm point of view, but it is not representative of the real scanned environment. These triangles are simply treated by the second algorithm, which eliminates any triangle that has a perimeter larger than a specified threshold.

2.3 Decimating

Finally, in order to reduce memory requirements, the mesh is simplified. The preliminary implementation currently used is a simplified version of the decimation algorithm presented in [14]. Mainly, we do not deal with what [14] refers to as "complex triangles" because our triangulation algorithm does not create any. Plus, instead of using the presented plane splitting technique for re-triangulating the holes, we simply "slide" triangles references from the eliminated vertex to the closest vertex among its neighbours. Triangles that were squeezed to flat lines by the operation are removed. Evaluating the decimation criteria on one point out of two, alternating on every consecutive pass seems to preserve a relatively good shape ratio among the triangles. Figure 6 shows some results. Note that even though the edge preservation criterion is not implemented yet, the mesh boundaries are still relatively faithful to the original mesh.

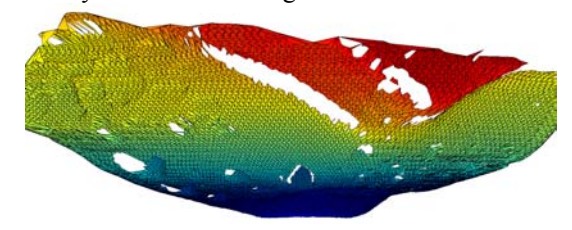


Figure 5 - Triangulation of a 49468 points scan, 1279 shadow triangles removed, 97623 triangles left

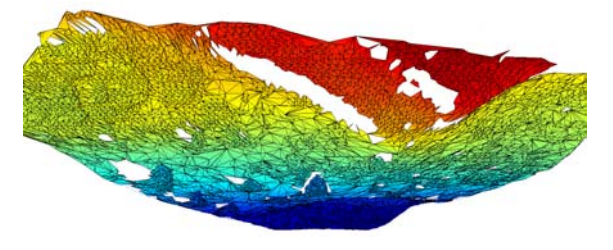


Figure 6 - Decimated triangulation, 23775 triangles left

3 SCAN REGISTRATION AND LOCALIZATION

A complete 3D reconstruction of a free-form surface requires acquisition of data from multiple viewpoints in order to compensate for the limitations of the field of view and for self-occlusion. In this paper, the reconstruction of the environment is performed in two steps. The first step consists of the assembly of the different views by estimating the rigid transformation between the poses from where each view was taken. The second step is the environment reconstruction, achieved by fitting a triangular mesh on each scan (as described above). Reconstructing a map of the environment in this way, allows us to conserve all information provided by scans. Thus our map of the environment is a set of scans mesh inter-related by the rigid transformation between scans.

3.1 Assembly of the different scans

In this step, different scans are registered in a common coordinate system. Since the coordinates of the viewpoint may not be available or may be inaccurate, the original ICP in Besl and McKay [4] may not converge to the global minimum. Thus, to assemble all views in the same coordinate frame, we used a variant of ICP, which differs from the original ICP by searching for the closest point under a constraint of similarity in geometric primitives. The geometric primitives used in this paper are the normal vector and the change of geometric curvature. The change of geometric curvature is a parameter of how much the surface formed by a point and its neighbours deviates from the tangential plane [3], and is invariant to the 3D rigid motion. Hence, in our algorithm, surface points are represented in \Re^7 . Coordinates of a point P on are $(x, y, z, n_x, n_y, n_z, K)$ where surface [x, y, z] are the Cartesian coordinates of P, $[n_x, n_y, n_z]$ are the coordinates of the normal vector and K is the change in curvature. Geometric primitives are used in matching by incorporating them in a 7D distance metric D_{α} of the form:

$$D_{\alpha}^{2}(p,q) = \sum_{i=1}^{7} \alpha_{i} (\lambda_{pi} - \lambda_{qi})^{2}$$

where the λ_i are coordinates of a 7D point and the α_i are the weights of each coordinate. Using this distance metric for finding the closest point is a combination of the 3D distance, the difference of the orientation of the normal vectors, and the difference of the change of curvature.

Our ICP algorithm can be summarize as follow: Let $P = \{p_1, p_2, ..., p_n\}$ and $Q = \{q_1, q_2, ..., q_m\}$ be

two sets of points in \Re^7 . The goal is to find a rigid transformation T=(R,T) composed of a rotation matrix R and a translation vector t that best aligns P to match Q. An informal description of the algorithm follows:

- Compute the normal vector and the change of curvature at each point of each cloud of points P, Q. Build a k-D tree representation of the cloud of points Q.
- 2. Initialize the matching process.
- 3. Repeat until the termination criterion is reached:
 - Compute the closest points $q_i = ClosestPo\, \mathrm{int}(p_i^k,Q)$. Where i=1,2,...,n, $q_i \in Q/D_\varepsilon(p_i^k,q_i) = \min(D_\alpha(p_i^k,Q))$. A k-D tree is used to speed up this search.
 - Discard undesired matches through statistical analysis of the distances, as described in Zhang [19].
 - Compute the rigid transformation T = (R,T) from the remaining matches, as in Zhang [19] and Besl and McKay[4].
 - Apply the rigid transformation to all points in $P: P_i^{k+1} = RP_i^k + t$ and rotate accordingly the normal vectors.
 - If the mean square error drops below a threshold, TERMINATE.

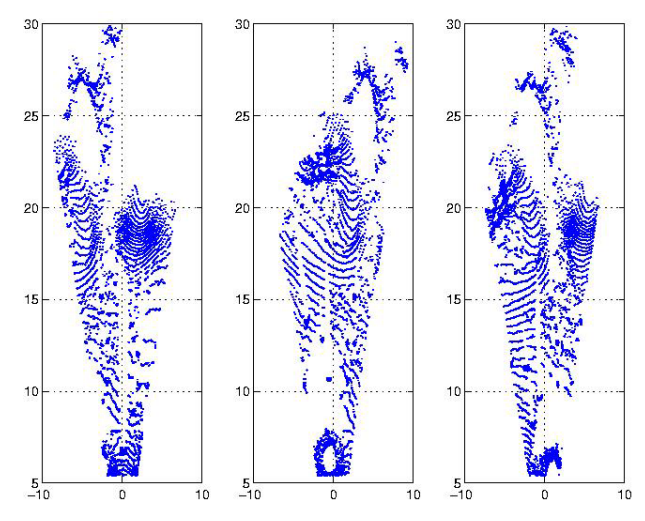


Figure 7 - Three terrain scans to be assembled

To illustrate the performance of different view assemblies, several views of the CSA's Mars

Emulation Terrain were taken from different viewpoints. Figure 7 illustrates three different views and Figure 8 gives the result of the assembled views using the above ICP algorithm.



Figure 8 - Assembled terrain scans in a single data set

Localization

The variant of ICP presented above is also used to localize the rover while navigating in the previously reconstructed environment. Given an estimation of the current position and orientation of the rover provided by our 3D odometry algorithm and a simulated LIDAR field of view model, one can extract a part of the map (sub-map), which can be visible from the current pose of the rover. Using ICP for matching the currently acquired scan with the sub map can refine the 3D odometry pose, thus improves the localization of the rover.

One important issue that need to be addressed is how to set the initial estimation of the pose of the rover in the global map of the environment. We are currently investigating two approaches: harmonic shape image [18] and spin-image [6] matching. Spin image is a local representation and does not preserve the continuity of the surface. Spin-image matching is time and memory consuming but provides point-to-point correspondence. Harmonic shape image preserves the geometric information, both shape and continuity, of the underlying surface. Its matching is a patch based matching, therefore doesn't provide point-to-point correspondence. According to the advantage and disadvantage of Spin image and harmonic shape image (see [6] and [18] for more details), we adopted the divide-and-conquer strategy. Our strategy consisted of applying first the harmonic shape images matching to find the local area where the rover is located in the global map and then use spin image matching only in this local area to find the correspondence between points and finally find the corresponding rigid transformation.

4 PATH PLANNING

In the context of long-range navigation, the path planners used on the CSA's Mobile Robotics Testbed concentrate on finding a global solution to travel between two points in natural settings while optimizing some cost function. The emphasis is on global path planning rather than local path planning and obstacle avoidance. The basic assumption is that a priori knowledge of the environment is available at a coarse resolution from orbital imagery/altimetry and is refined using local range sensing of the environment. The composite environment model (coarse with refined portions) is then used to plan a path that will be generally safe and that will be updated periodically as new environment data is available.

Previous CSA work used DEM from which a separate traversability map was created based on local slope. The traversability map was itself represented in a quadtree structure on which a graph search algorithm was applied to find a safe path [8] [17]. While this approach worked, it required a separate structure for the terrain data and traversability map, which forced the update of the traversability map and the quad-tree structure when the DEM was modified.

The use of irregular triangular mesh to represent terrain data allows us to integrate the terrain representation with the path planning easily. To do so, an undirected weighted graph representing the triangles connectivity is created where the triangles are the vertices of the graph and a triangle connectivity to its neighbours are represented as edges. The JGraphT Java Library [12], available freely on the Web, has been used to implement the graph structure and functions.

The edge weight or cost is defined by providing a function that yields a cost based the distance between the vertices, slope of the edge, slope of the triangles, mean altitude, or a combination of these to yield the cost associated with moving from one triangle to another. The cost function is associated to the edges at the graph creation, but the actual cost computed only on request.

Once the graph is constructed, a path between the current rover location and a destination can be planned. The process involves four steps:

1) Finding the two triangles where the current location and the destination lie;

- Applying the Dijkstra's shortest path search algorithm (provided in *JGraphT*) to find a safe path:
- Creating a list of waypoints based on the path found;
- 4) Generating a simplified trajectory from the list of waypoints.

Applying the Dijkstra's shortest path algorithm on the triangle connectivity graph from the current location to the destination triangles produces a list of edges along the path. This list is used to create a list of the triangles to be traversed. Finding the center of each of the triangles making the path yields a list of waypoints.

The trajectory defined by the waypoints list has often a "saw tooth" look, which makes it difficult to follow for the robot guidance. In order to alleviate the problem, the waypoint list is processed in order to remove unnecessary waypoints while maintaining the resulting trajectory on safe ground. Figure 9a and Figure 7b show the effect of the trajectory simplification.

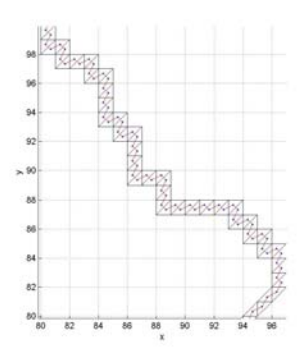


Figure 9a - Trajectory generated using waypoint list

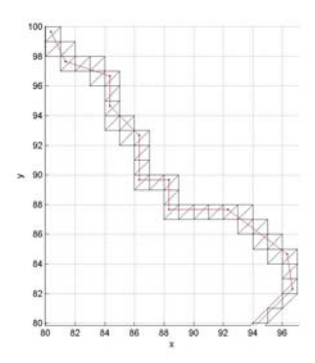


Figure 7b - Trajectory after simplification

Various cost functions have been tested with the path planner. For example, Figure 10 shows the result for planning a path from location (15.0, 5.0) to (80.0, 100.0) (in meters) using a cost function that takes into account distance and slope.

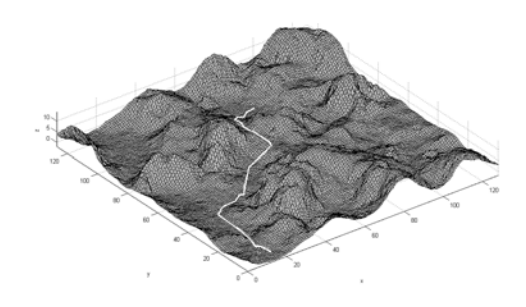


Figure 10 - Trajectory minimizing slope and distance travelled

5 ROVER GUIDANCE

The usage of a scanning lidar for terrain sensing results in a concept of operation slightly different from the more common schemes using stereo pairs. Indeed the scanning lidar used on the CSA's Mobile Robotics Test-bed typically takes on the order of one or two minutes to perform a terrain scan but it has a sensing range of over a kilometre. As a result, the terrain is not imaged continuously. It is rather imaged using snapshots taken at discrete intervals. Obviously, since the lidar is located near ground level, the effective range of the measurements is typically not on the order of kilometres but of a few tens of meters. Consequently, the rover has the ability to plan path segments on the order of 20 to 30 meters and does not rely on environment sensing while moving along these path segments. It has, therefore, been necessary to develop guidance software that can keep the robot precisely on the planned trajectory. The proposed rover guidance has two mains parts: 3D odometry and autonomous motion controller.

5.1 3D Odometry

The first step to ensure that the robot does not deviate from the planned trajectory is to provide accurate knowledge of its position. This task can be accomplished by fusing odometry, inertial, and also absolute heading data. In this system, the robot odometry is combined with a solid-state IMU (inertial measurement unit) sensor to provide inertial navigation with 3D odometry. An absolute heading sensor, a digital compass TCM2 from PNI Corporation provides absolute orientation in Yaw (in Mars exploration, this sensor could easily be replaced by a sun sensor).

The angular velocities measured by the IMU are integrated to form the orientation in SO(3) using the quaternion formulation. Once the orientation is

obtained, the 3D odometry can be easily obtained by incorporating the robot odometry based on the wheel movements. However, data drifting in 3D odometry is fundamental. Correction or re-calibration is needed regularly. In the system, the gravitational vector is extracted from the three-axis acceleration signals provided by the solid-state IMU. The gravitational vector is used to correct the pitch and roll generated by the 3D odometry. Since the gravitational acceleration vector is very noise, particularly when the robot rolls over small rocks, a Kalman filter based on quaternion in SO(3) is used. Finally, the yaw correction is performed by the absolute heading sensor, which is activated every time the robot stops because the compass data is not reliable when the robot motors are running due to the electromagnetic interference.

Table 1 lists three different IMU with their cost, random walk, and the resulting orientation drifting. The first row corresponds to the IMU used in this system. The second and third rows correspond to two IMU suggested by Durrant-Whyte [16]. The angular velocity random walk is a key indicator that represents the original performance of the IMU. In general, it is proportional to the standard deviation of the angular velocity measurement noise. A big random walk is always associated with a low price and a high orientation drifting for a given integration algorithm. In view of the first two rows, the random walk in the first row is about 4.5 times higher than that in the second row. But the orientation drifting in the first row is only twice as much as the second row. This indicates the effectiveness of the quaternion-based integrator developed at CSA.

Table 1 - Comparison of drift for different IMU

IMU	Price (US\$)	Random Walk (deg/hr1/2)	Orientation drifting
IMU300 (Crossbow)	3K	< 2.25	3 deg in 10 minutes 6 deg in 15 minutes
ISIS-IMU (Inertial Science)	10K	<0.5	3 deg in 15 minutes
DMARS-I (Inertial Science)	30K	<0.02	0.5 deg in 15 minutes

Experimental results of the 3D odometry with the gravitational vector based pitch and roll correction are illustrated in Figure 11. The dashed line represents the planned trajectory that covers an 8m by 8m region. The solid line represents the actual robot positions in 3D. In the far edge when x is around 10m. The vertical difference between the solid line and the dashed line is

due to the fact that the commanded trajectory does not take into account a rise in the physical terrain. After completion of the closed trajectory, the total travelled distance is approximately 32m. The position drifting in z only amounts to 3.1cm. This error is indicative of the portion of the error due to drift of the IMU. In contrast, the position drifting by using the robot odometry alone (based on wheel movements) amounts to 9.3m for the same trajectory, resulting from the significant orientation error caused by wheel slippage.

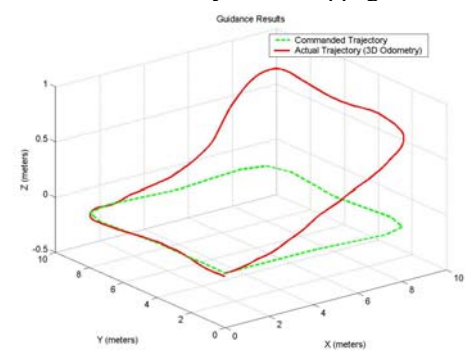


Figure 11 - Experimental results from 8m x 8m outdoors traverse

5.2 Autonomous Motion Controller

The developed motion control is based on a discontinuous state feedback control law initially proposed by Astolfi [2].

Experimental results in an outdoor 3D environment (see Figure 1) show the robustness and the stability of the developed path following approach. The Figure 12 illustrates an 8m by 8m square-shaped reference path following result. A part on the path was on a slope and during the autonomous motion execution, artificial perturbations were induced twice as show in Figure 13. This figure shows that the rover can robustly, quickly and smoothly recover the path. During our tests with and without perturbations, physical error at the end of the motion was always negligible (about few centimeters in position and few degree in orientation) and it is due essentially to the wheels slippage and the gyroscope drift. For example, the errors of the test in Figure 12 and Figure 13 were on the order of 15 centimeters in position and 3.3 degree in orientation. The physical error in position was measured by putting marks on the ground, while an onboard compass (in rest state) provided the orientation error. The same trajectory was executed without perturbation and the result is shown in Figure 11. Others trajectory such as eight-shape (Figure 14, Figure 15) and closed-spiralshaped (Figure 16, Figure 17) have been also executed. All those results illustrate the precision and the performance of the proposed autonomous motion controller and the 3D odometry based localization.

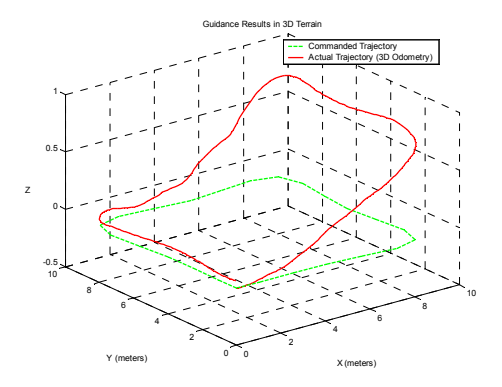


Figure 12 - Square-shaped path following with artificially induced perturbations: in 3D

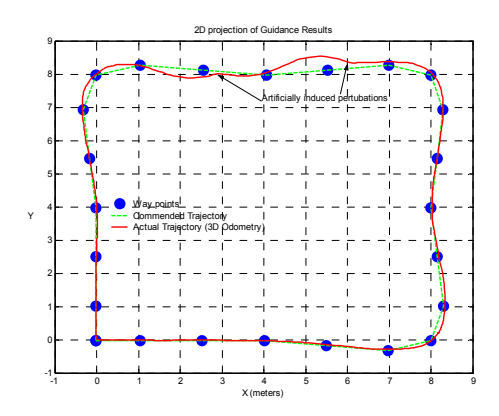


Figure 13 - Square-shaped path following with artificially induced perturbations: 2D projection

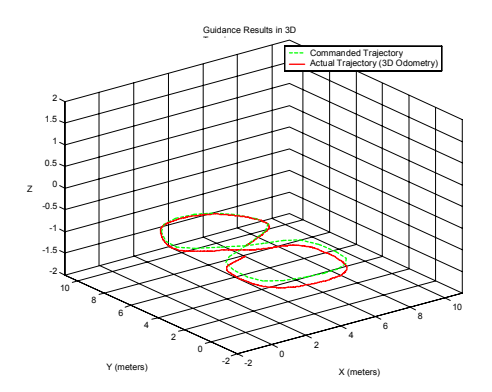


Figure 14 - Eight-shaped trajectory execution

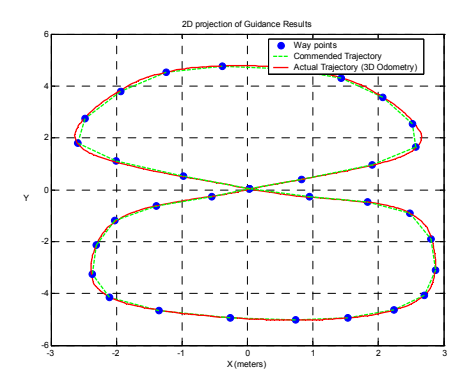


Figure 15 - Eight-shaped trajectory 2D projection

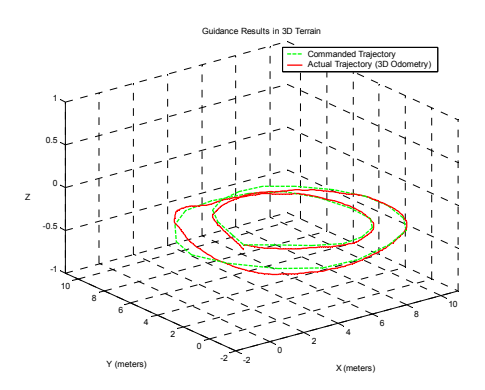


Figure 16 – Closed spiral-shaped trajectory execution

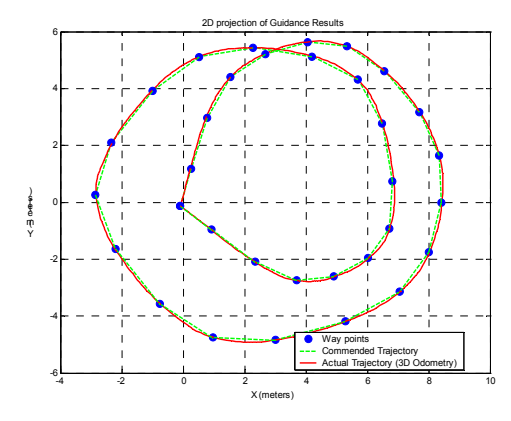


Figure 17 - Spiral-shaped trajectory 2D projection

6 CONCLUSION

This article has presented and discussed the advantages of map building via triangulation and path planning through an irregular triangulated mesh, and the algorithms used for rover guidance in outdoor terrain. Experimental results demonstrate that the terrain-modelling scheme can be used to model natural terrains efficiently and is directly usable for path planning using a variety of cost functions. The robustness and stability of the rover guidance in rough 3D terrain is demonstrated. Closed trajectories of up to 50 meters have been executed successfully in natural terrain even in the presence of external disturbances. Position errors

on the order of less than 1% of the total distance travelled have been observed in many cases.

Future work will focus on Simultaneous Localisation and Mapping, increased autonomy and longer-range navigation. Traverses on the order of 100 metres and more will require the ability to stitch maps together and to perform map-based localisation.

7 REFERENCES

- [1] A. P. Aguiar, A. N. Atassi, A. M. Pascoal, "Regulation of a Nonholonomic Dynamic Wheeled Mobile Robot with Parametric Modeling Uncertainty using Lyapunov Functions", Proc. of CDC 39th IEEE Conf. On Decision and Control, Sydney, Australia, December 2000.
- [2] A. Astolfi, "Exponential stabilization of wheeled mobile robot via discontinuous control", Journal of Dynamic Systems Measurement and Control, March 1999, pp. 121-126
- [3] K.-H. Bae and D. D. Lichti. Automated registration of unorganised point clouds from terrestrial laser scanners. In The 20th ISPRS Congress, Istanbul, Turkey, July 2004.
- [4] P. J. Besl and N. D. McKay. Amethod for registration of 3-d shapes. IEEE Trans. on Pattern Analysis and Machine Intelligence, 14(2):239-256, 1992.
- [5] T. Estlin, F. Fisher, D. Gaines, C. Chouinard, S. Schaffer, I. Nesnas, "Continuous Planning and Execution for an Autonomous Rover," Proceedings of the Third International NASA Workshop on Planning and Scheduling for Space, Houston, TX, October 2002.
- [6] A. Johnson. Spin-Image: a representation for 3-D surface matching. Ph.D thesis, Carnegie Mellon University, 1997.
- [7] S. Lacroix, I-K Jung, J. Gancet, J-J Gonzalez-Barbosa, "Towards long range autonomous navigation", *Proc. of 7th ESA Workshop on Advanced Space Technologies in Robotics and Automation*, Noordwijk, the Netherlands, November 2002.
- [8] C. Lange, P.Allard, E. Dupuis, Y. Gonthier, "Unified Facility for the Development, Integration and Testing of Autonomous Navigation Schemes for Planetary Exploration", *Romansy Conference, Montreal Canada*, June 2004.
- [9] J.E. Lloyd, "ConvexHull3D", http://www.cs.ubc.ca/spider/lloyd/java/convexhull3d.html

- [10] M. Maurette, "Mars Rover Autonomous Navigation", *Autonomous Robots*, v. 14, pp.199-208, 2003
- [11] D.P.Miller, T.Hunt, M.Roman, S.Swindell, and L.Tan & A.Winterholler, "Experiments with a Long-Range Planetary Rover", *Proc. of 7th International Symposium on Artificial Intelligence, Robotics and Automation in Space*, Nara, Japan, May 2003.
- [12] B. Naveh and al. "JGraphT", http://jgrapht.sourceforge.net
- [13] L. Pedersen, R. Sargent, M. Bualat, C. Kunz, S. Lee, and A. Wright, "Single-Cycle Instrument Deployment for Mars Rovers", *Proc. of 7th International Symposium on Artificial Intelligence, Robotics and Automation in Space*, Nara, Japan, May 2003.
- [14] W.J. Schroeder, J.A. Zarge, and W.E. Lorensen, "Decimation of Triangle Meshes", Computer Graphics (SIGGRAPH '92 Proceedings), Vol. 26, No. 2, July 1992, pp. 65-70.
- [15] C. Urmson, R. Simmons, I. Nesnas, "A Generic Framework for Robotic Navigation," *Proceedings of the IEEE Aerospace Conference*, Montana, March 2003.
- [16] H. Durrant-Whyte, "A critical review of the state-of-the-art in autonomous land vehicle systems and technology," Sandia Report SAND2001-3685, Sandia National Laboratory, Albuquerque, NM, 2001.
- [17] S. Gemme, J. N. Bakambu and I. M. Rekleitis
 " 3D Reconstruction of Environments for
 Planetary Exploration", Second Canadian
 Conference on Computer and Robot Vision
 (CRV 2005), Victoria, BC, Canada, pages
 594--601, May 9-11, 2005
- [18] Dongmei Zhang. Harmonic Shape Images: A 3D Free-form Surface Representation and its Application in surface Maching. Ph.D thesis, Carnegie Mellon University, 1999
- [19] Z. Zhang. Iterative point matching for registration of free-form curves and surfaces. Int. Journal of Computer Vision, 13(2):119-152, 1992.